Int. J. Environ. Sci. Technol. (2016) 13:1159–1168
DOI 10.1007/s13762-016-0958-7

ORIGINAL PAPER

The response of reworked aerosols to climate through estimation of inter-particle forces

A. Assadi Langroudi[1] · **I. Jefferson**[2]

Received: 10 February 2015 / Revised: 2 November 2015 / Accepted: 10 February 2016 / Published online: 24 February 2016

Abstract This paper describes the first use of inter-particle force measurement in reworked aerosols to better understand the mechanics of dust deflation and its consequent ecological ramifications. Dust is likely to carry hydrocarbons and micro-organisms including human pathogens and cultured microbes and thereby is a threat to plants, animals and human. Present-day global aerosol emissions are substantially greater than in 1850; however, the projected influx rates are highly disputable. This uncertainty, in part, has roots in the lack of understanding of deflation mechanisms. A growing body of literature shows that whether carbon emission continues to increase, plant transpiration drops and soil water retention enhances, allowing more greenery to grow and less dust to flux. On the other hand, a small but important body of geochemistry literature shows that increasing emission and global temperature leads to extreme climates, decalcification of surface soils containing soluble carbonate polymorphs and hence a greater chance of deflation. The consistency of loosely packed reworked silt provides background data against which the resistance of dust's bonding components (carbonates and water) can be compared. The use of macro-scale phenomenological approaches to measure dust consistency is trivial. Instead, consistency can be measured in terms of inter-particle stress state. This paper describes a semi-empirical parametrisation of the inter-particle cohesion forces in terms of the balance of contact-level forces at the instant of particle motion. We put forward the hypothesis that the loss of Ca^{2+}-based pedogenic salts is responsible for much of the dust influx and surficial drying pays a less significant role.

Keywords Dust · Deflation · Menisci · Pedogenic · Inter-particle forces

Introduction

The World Health Organization estimated an annual 1.3 million deaths as a result of air pollution, the most significant type of which is particulate matter (USEPA 2013) with an estimated mean annual global flux of 1020–2070 Tg (Miller et al. 2004; Ginoux et al. 2004) and 1–3.6 Pg yr^{-1} mobilisation rate (Maher et al. 2010), out of which 1500 Tg settles on land when physio-chemical processes favour the down flux (Shao et al. 2011). The resistance of dust to deflation (i.e. saltation) has been numerically modelled in several works (Smalley 1970; Marticorena et al. 1997; Alfaro et al. 1998; Creyssels et al. 2009, etc.) and experimentally measured—at macro-scale—in terms of flux-crust strength (Goossens 2004). Yet, the mechanics of accumulated dust transformation from unstable to metastable state is yet poorly known (Svirčev et al. 2013), in part due to the hardship in measurement of *fluid threshold*. The threshold is a function of both gravitational and inter-particle cohesion forces that oppose the particle lifting (Bagnold 1941). A semi-empirical method has been adopted here to explore the relative

Electronic supplementary material The online version of this article (doi:10.1007/s13762-016-0958-7) contains supplementary material, which is available to authorized users.

✉ A. Assadi Langroudi
A.AssadiLangroudi@uel.ac.uk

[1] The School of Architecture, Computing and Engineering, University of East London, Docklands, London, England, UK

[2] College of Engineering and Physical Sciences, University of Birmingham, Birmingham, England, UK

significance of water menisci and chemical cementation—as two components of the *fluid threshold*—through evoking the well-established physical principles and approximating the Newtonian forces at particle level.

Dust initially emits from continental areas over periods of semi-aridity and settles when wind intensity decreases over moist and rough lands. Deposited dust then combines with electrically charged minerals (including clay and ions) to develop metastable open structures, lent by a suite of Newtonian forces including skeletal, weight, hydrostatic, hydrodynamic and buoyant. Newtonian forces balance capillary and cementation forces (Santamarina 2003). For a wind erosive force greater than the sum of capillary–cementation forces combined (*fluid threshold*), destabilisation in dust's structure initiates which potentially leads to deflation. For the relative significance of *fluid threshold* components to be quantified, inter-particle forces need to be measured.

The research into explicit links between macro-scale actions (e.g. water content, net stress) and microscopic features (e.g. contact forces) has been the subject of numerous works, perhaps beginning with the work of Dantu (1957) on mechanisms of load transfer in granular material using optically sensitive discs. Inter-particle forces were expressed by some workers in terms of average stress tensor (Cundall and Strack 1983; Thornton and Barnes 1986), although it might be argued as force transmission in granular packings is known to be peculiar and above all, very inhomogeneous. The latter shortfall was filled later in a number of models including the Claudin et al. (1998). Much of the parametrisation equations for inter-particle force has been reported in the aeolian saltation theory literature in an attempt to determine threshold stress for particles lifting into atmosphere. For example, Cornelis et al. (2004) formulated (Eq. 1) the inter-particle force (F_{ip}) as sum of London dispersion force (K_{vdw} proportionality coefficient times diameter), 'wet' bonding force (a function of surface tension σ, diameter d and matric suction ψ_m) and effective gravitational force (a function of effective density $\rho_s - \rho_f$ and gravitational moisture content ω). Our recent findings (Assadi and Jefferson 2013) lend some degrees of uncertainty to the latter formulation since first, the model does not consider the implications of packing's change—and double porosity—and secondly, the model is based on three-phase solid–air–liquid systems and excludes chemical cementation forces as a component of cohesive inter-particle force. In the more recent (Ravi et al. 2006) study, emphasis was kept on soil water retention (Eq. 2) in clean granular systems considering the water retention properties. They accommodated a van den Waals force $\beta_c d$ component together with the capillary force in their equation but did not take the implications of chemical cementation forces into account.

$$F_{\mathrm{ip}} = K_{\mathrm{vdw}} \cdot d + \frac{K_{\mathrm{AC}} \cdot \sigma^2 \cdot d^2}{|\psi_m|} + (1+\omega)K_{\mathrm{G}}\left(\rho_s - \rho_f\right) g d^3 \tag{1}$$

$$F_{\mathrm{ip}} = d\left[\pi\left(\frac{c}{\rho_w \sigma}\left(\frac{RT}{M}\right)^{-b}\left(\ln\frac{RH}{100}\right)^{-b} - \frac{y}{2}\right)\right]\frac{RT}{M} \times \ln\left(\frac{RH}{100}\right) + \beta_c d \tag{2}$$

Ishizuka et al. (2008) further extended the formulations and introduced σ_m, which is a function of the soil plastic pressure, hardness of ground or crust binding force. They then reported a direct relationship between hardness function, $\rho_b \Omega / m = \sigma_m$ (normalised against mass of impacting particles) and rate of dust emission (Eq. 3).

$$\tilde{F}(D_i, D_s) = c_y\left[(1-\gamma) + \gamma\frac{\rho_m(D_i)}{\rho_f(D_i)}\right]\frac{\hat{Q}g}{u_*^2 m}\left(\rho_b \eta_{fi} \Omega + \eta_{ci} m\right) \tag{3}$$

One important milestone in mechanics of granular materials at grain scale was the inception of discrete element method (DEM) introduced by Cundall and Strack (1979), which was followed by a thread of statistical approaches to measure inter-particle forces (Guo and Zhao 2013; Ostojic et al. 2006). Discrete models, however, lack in their reliance on computational power, forcing workers to resort to enlarging the particles and calibrating the model, and in the use of spheres and ellipsoids, which leads to negligence of the grain angularity (Andrade and Tu 2009). The restriction of direct measurement technologies in measuring contact forces within colloidal suspensions, motivates the use of simple principles of physics to capture the particle-level phenomena.

This paper describes a semi-empirical parametrisation of the inter-particle cohesion forces in a loosely cemented aeolian silt in terms of the balance of contact-level forces at the instant of particle motion. Much of the links between the macro- and micro-parameters are developed and presented for a homogeneous two-dimensional analogy of assemblies of spheres, an extension of the well-known Santamarina (2003) equation.

The simplicity of the method offers the chance to reader to replicate the experiments. Despite assuming particles as mono-dispersed spheres, which is a strong assumption, the process is able to represent the macroscopic behaviour of aerosol materials under relatively well-controlled and homogeneous conditions, not untypical to much of the $PM_{10\text{–}20}$ aeolian deposits.

Materials and methods

Testing materials

Silt-sized quartz particulate matter (PM) was artificially produced through grinding dry clean (washed with Calgon: 33 g sodium hexametaphosphate and 7 g sodium carbonate in 1 l distilled water) 1.15 mm (peak on 0.5–0.6 mm) in diameter Leighton Buzzard Lower Greensand in a Siebtechnik 800W TS1000 disc mill (Assadi et al. 2014) followed by gravity sedimentation using Stoke's law to omit the sub-2 µm and >63 µm tails as explained in Lamb (1994) and initially practiced in similar fashion by Assallay (1998). Grinding input (energy duration) was tailored, via try and error, to generate a peak on 10–20 µm size of the ground sand. Mode size distribution was captured using a Sympatec laser diffraction machine using a 1.544 refractive index at a 99.73 % degree of confidence (O'Hara-Dhand et al. 2013). Ground sand was crumbled and mixed dry with kaolinite (Polwhite-E containing 74–80 % kaolin, 2–3 % montmorillonite, 5–12 % feldspar, 5–15 % mica and 1–2 % quartz) and anhydrous sodium carbonate at Silt:70|Clay:10|Carbonate:20 per cent by weight proportion to produce a benchmark sub-63 µm dry saline dust material. Under controlled ambient conditions (relative humidity and temperature), dust was pluviated into a 75-mm oedometer ring at a constant rate and freefall height. Distilled water was finely sprayed on the surface of freshly deposited dust (for every 2 mm high dust column). Trimmed aeolian specimen was axially loaded to a 12.5-kPa seating pressure before a 48-h drying course at 75–85 °C temperature. To replicate the reworking process, a dilute 0.4 M (110.98 g/mol modal mass) calcium chloride solution (pH 8.0) was introduced to the dry specimen from the lower drain point for 8 h before a subsequent drying at 75–85 °C. Chemical curing was repeated two more times to generate a combination of aragonite and calcite carbonates within the dust structure [verified through X-ray diffraction and energy-dispersive X-ray spectroscopy in Assadi (2014)]. The reworked dust product was eventually dried to 0.4 % hygroscopic water content and a void ratio of 1.19–1.41 (unit weight of 11.0–12.1 kN/m^3), not untypical of much of the globally distributed deposited silt-sized aerosols. Mode size distribution of testing material is illustrated in Fig. 1.

Testing procedures

Thirteen free oedometer tests (ASTM 2014; BS 1990) were performed on identical specimens, through wetting (from the lower drain point by the act of capillary) for 0.75, 1.5, 2, 2.25, 3, 5, 7, 10, 80, 160, 320, 720 and 1527 min. Water content was recorded at the end of each experiment. The fourteenth specimen was assembled in the oedometer cell, equipped with a graduated pipette that passed vertically through the flanged top disc to the bottom of the chamber. In an attempt to examine the implications of groundwater flow at grain scale, a steady-state flow (70 min) followed by hydrostatic condition was simulated under a net stress slightly lower than the swelling pressure. The specimen's height (and hence void ratio) was recorded against the wetting time upwards from 0 s at intervals of 10 s.

Model development

Skeletal force

A simple soil fabric model (i.e. domain) was adopted to approximate the skeletal force at grain level from net stress. d-sized cubic clusters were aligned in chains along three Cartesian axes. Each column of clusters was surrounded by a neighbouring column of 'void' d-sized cubes, representing the macro-pores (Fig. 2). To build a suite of solid–void combinations, void cubes were allowed to accommodate sub-d-size solid cubes. Also, solid cubes were allowed to accommodate sub-d-size void cubes. Sub-d-size void cubes represent micro-pores. The effective area (A_e) was defined as solid occupancy in every $2d$-sized square area. The effective area was considered as the region of solids that carry the effective stress. Over 50 solid–void combination cases were collated into an inventory of void ratio versus effective area. The 'cubic expression' was converted into a 'spherical expression' by presuming equal surface areas in vertical projection (Eq. 4).

$$d_{squ}^2 = \frac{1}{2}4\pi\left(\frac{d_{sph}}{2}\right)^2 : d_{squ} \approx d_{sph}\sqrt{\frac{\pi}{2}} \quad (4)$$

where d_{squ} is width of a cube surrounding a sphere particle of d_{sph} in diameter. In two dimensions, skeletal force at grain scale was expressed as,

$$F_{(N)skel} = \sigma' \cdot f\{e, d\} \quad (5)$$

where $f\{e, d\}$ is a function of void ratio (e) and particle mean diameter (d). The built e–A_e inventory (partly reported in Table 1) was inputted into a nonlinear regression calculation using the Levenberg–Marquardt algorithm, to express the $f\{e, d\}$ in the exponential form of Eq. 6.

$$f\{e, d\} = \frac{\pi}{2}d^2 \cdot A \cdot \exp(B \cdot e + C\sqrt{e}) \quad (6)$$

where A, B and C are fitting parameters. Figure 2 shows an example of the defined simple soil fabric model.

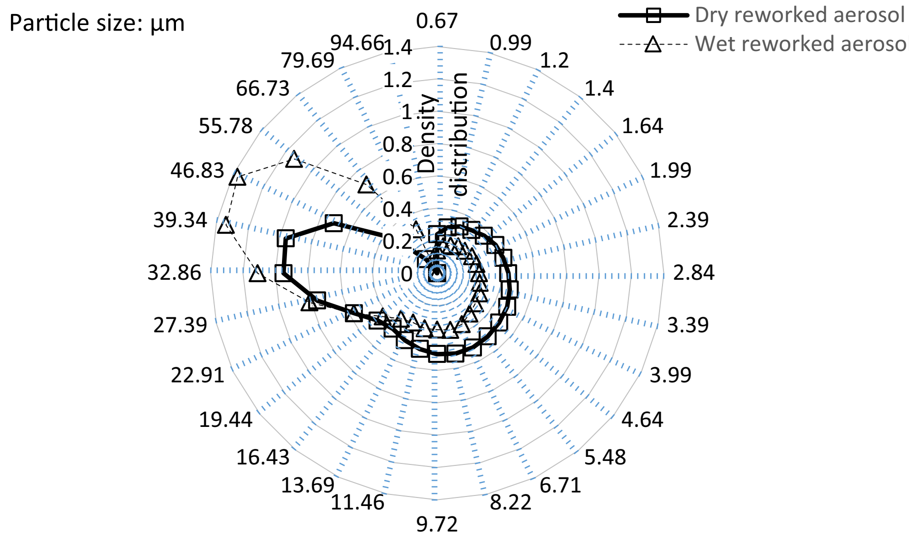

Fig. 1 Mode size distribution of testing aerosol identical specimens

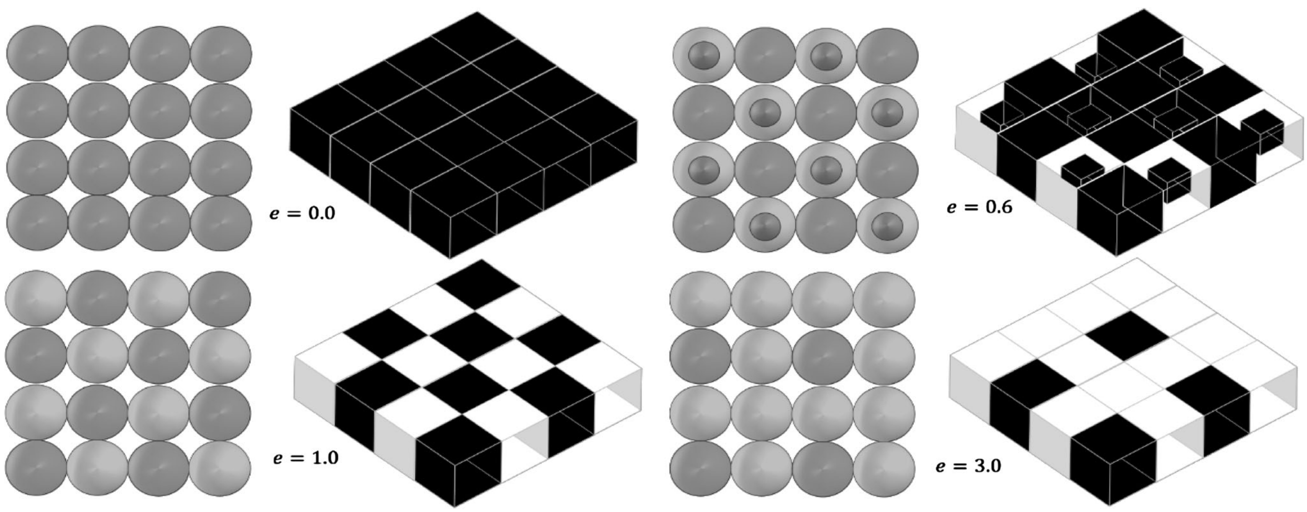

Fig. 2 Effective bearing area as a function of packing state

Buoyant, weight and hydrostatic force

For wetting times less than the time needed for the waterfront to travel the soil column to mid-height, the dry state of grains was imitated with zero buoyant, hydrostatic and hydrodynamic force. Within the framework of physical principles accepted to date,

$$B = \frac{1}{6} \times \pi \times \gamma_w \times D_{50}^3 \quad \text{for } t > {}^{t_1}/_2 \tag{7}$$

$$U = 0.5\left(\frac{\dot{H}_i}{2} + \dot{H}\right) \cdot \rho_w \cdot 4\pi \cdot \left(\frac{D_{50}}{2}\right)^2 \quad \text{for } t \geq t_1 \tag{8}$$

$$W = \sum W_j = \frac{\dot{H}_i}{2D_{50}} \times \frac{1}{6} \times \pi \times \gamma_w \times G_s \times D_{50}^3 \tag{9}$$

where 'B' is the buoyant force, t_1 is the time elapsed between the arrival of the water at the top of the specimen and the beginning of the percolation at the lower drain point, 'U' is the hydrostatic force, $\dot{H}_i$ is the specimen height (varied), $\dot{H}$ is water overhead, and 'W' is the weight force. The weight force was assumed compressive and aligned with the gravity direction. The buoyant force was assumed tensile, reducing either the skeletal or weight forces. Volumetric contraction was mirrored in declining timed trend of hydrostatic force.

Hydrodynamic force

The Stoke's law at low Reynolds numbers (Bear 1972; Graf 1984; Santamarina 2003) was here utilised to express the hydrodynamic force as in Eq. 10.

$$D = 3\pi \times \mu \times V \times d = 3\pi \times 10^{-3} \times D_{50} \times \frac{K_i \times i_i}{n_i} \tag{10}$$

Table 1 Selective outputs from the DE model

Void ratio	Effective area (cubic expression) A_e	Effective area (spherical expression) A_e	Mean normal contact force
0.000	$4\ d^2$	$(\pi/2)\ 4d^2$	$(\pi/2)\sigma'\ 4\ d^2$
0.286	$2.67\ d^2$	$(\pi/2)\ 2.67\ d^2$	$(\pi/2)\sigma'\ 2.67\ d^2$
0.330	$3\ d^2$	$(\pi/2)\ 3\ d^2$	$(\pi/2)\sigma'\ 3\ d^2$
0.385	$2.44\ d^2$	$(\pi/2)\ 2.44\ d^2$	$(\pi/2)\sigma'\ 2.44\ d^2$
0.600	$2.5\ d^2$	$(\pi/2)\ 2.5\ d^2$	$(\pi/2)\sigma'\ 2.5\ d^2$
0.800	$2.22\ d^2$	$(\pi/2)\ 2.22\ d^2$	$(\pi/2)\sigma'\ 2.22\ d^2$
1.000	$2\ d^2$	$(\pi/2)\ 2\ d^2$	$(\pi/2)\sigma'\ 2\ d^2$
1.250	$1.67\ d^2$	$(\pi/2)\ 1.67\ d^2$	$(\pi/2)\sigma'\ 1.67\ d^2$
1.286	$1.625\ d^2$	$(\pi/2)\ 1.625\ d^2$	$(\pi/2)\sigma'\ 1.625\ d^2$
1.670	$1.5\ d^2$	$(\pi/2)\ 1.5\ d^2$	$(\pi/2)\sigma'\ 1.5\ d^2$
2.200	$1.25\ d^2$	$(\pi/2)\ 1.25\ d^2$	$(\pi/2)\sigma'\ 1.25\ d^2$
2.600	$1.11\ d^2$	$(\pi/2)\ 1.11\ d^2$	$(\pi/2)\sigma'\ 1.11\ d^2$
3.000	$1\ d^2$	$(\pi/2)\ 1\ d^2$	$(\pi/2)\sigma'\ 1\ d^2$
>3.000	$1\ d^2$	$(\pi/2)\ 1\ d^2$	$(\pi/2)\sigma'\ 1\ d^2$

where K_i is the full-function hydraulic conductivity at wetting time $t = t_i$, n_i is the porosity, D_{50} is the mean particle size, and i_i is the hydraulic gradient as expanded in Eq. 11 for three scenarios (1) $0 \leq t < {}^{t_1}/_2$ immediately after wetting, (2) ${}^{t_1}/_2 \leq t < t_1$ steady-state flow and (3) $t \geq t_1$ constant head state.

$$\forall\, 0 \leq t < {}^{t_1}/_2 \Rightarrow 0 \tag{11}$$

$$\forall\, 0 = t \Rightarrow i = \frac{\Delta H}{H} = \frac{H_w - \left(t_{SL} + \frac{\dot{H}_i}{2}\right)}{\dot{H}_i/2}$$

$$\forall\, t = {}^{t_1}/_2 \Rightarrow i = \frac{\Delta H}{H} = \frac{H_w - \left(t_{SL} + \frac{H'_i}{2}\right)}{\dot{H}_i/2}$$

$$\forall\, {}^{t_1}/_2 < t < t_1 \Rightarrow i = \frac{\Delta H}{H} = \frac{H_w - \left(t_{SL} + 3/4H'_i\right)}{{}^3/_4 H'_i}$$

$$\forall\, t = t_1 \Rightarrow i = \frac{\Delta H}{H} = \frac{H_w - \left(t_{SL} + H''_i\right)}{H''_i}$$

$$\forall\, t > t_1 \Rightarrow i = \frac{\Delta H}{H} = \frac{H_w - \left(t_{SL} + \dot{H}_i\right)}{\dot{H}_i}$$

where t_{SL} is the height of the oedometer lower porous disc, H''_i is the height of the specimen at $t = t_1$, H'_i is the height of the specimen at $t = {}^{3t_1}/_4$, and H_w is the height of the water column in the oedometer chamber.

The full-function hydraulic conductivity was estimated using Darcy law for the measured degree of saturation, void ratio and hydraulic gradient, assuming a linear relationship between wetting front advancement and wetting time.

Capillary force

Depending on the degree of saturation, unsaturated soils follow either pendular or funicular regimes corresponding to low or high level of water contents, respectively. At both states, liquid bridges form between particles. Liquid bridge units impact the soil structure through developing tensile forces at particle level. The geometry of the liquid bridge is often described by the Laplace–Young equation. In this context, tensile forces depend on inter-particle separation distance, liquid bridge curvature and particle radii. A history of early to recent studies on liquid bridges is brought in Harireche et al. (2013). Here, the funicular-state capillary force (F_{cap}) was estimated using the Laplace's differential equation for unique curvature radii (Santamarina 2003) as shown in Eq. 12.

$$F_{cap} = \frac{T_s}{d_{pore}} \times 0.5 \times \left[4\pi\left(\frac{D_{50}}{2}\right)^2\right] = \frac{\pi \times D_{50}^2 \times T_s}{2d_{pore}} \tag{12}$$

where d_{pore} denotes the mean pore size (i.e. corresponding with the D_{50}) and T_s is the surface tension for water–air interface in ambient conditions (Fredlund and Rahardjo 1993). The mean pore diameter here was calculated using the Arya–Paris pedo-transfer function (Arya et al. 1999; Arya and Paris 1981, 1982; Haverkamp and Parlange 1982). The function involves dividing the cumulative particle-size distribution curve into a number of fractions, each representing a mean pore radius (r_i) and water pressure head (ψ_i). Arya and Paris (1981) proposed a nonlinear expression to relate the pore radius (r_i) to the mean particle radius (R_i):

$$r_i = R_i \cdot \left(\frac{4 \cdot e \cdot n_i^{1-\alpha}}{6}\right)^{0.5} \tag{13}$$

where e is the void ratio and n_i is the number of particles in each size fraction derived from:

$$n_i = \frac{W_i}{\left(\frac{4}{3}\pi \cdot R_i^3\right) \cdot \frac{W_s}{V_s}} = \frac{3W_i}{4\pi \cdot R_i^3 \cdot \gamma_s} \tag{14}$$

where W_i is the solid mass (per unit sample mass) associated with R_i (i.e. in each given size fraction), in a way that the sum of the W_i is unity. γ_s is the particle density taken equal to $G_s \cdot \gamma_w$, and α_i is the 'scaling factor' (i.e. tortuosity factor). Within the adopted framework, the radius of a given pore is a factor of the mean radius of particles surrounding that pore, in a soil of certain void ratio and specific gravity. For a domain made up of a mesh of equally dimensioned squares, both particles (solids) and pores (voids) can be modelled as squares, the number of which is assumed equal. Hence, the population of the particles can be deemed equal to the population of pores. A sample of calculations is reported in Appendix 1 for interested readers (i.e. supporting document).

The Mikami et al. (1998) pendular-state capillary force formulation for smooth sphere pairs is herein practiced, with moderation. Formulation has been inferred from numerical solutions of Laplace–Young equation together with geometric considerations. The same relation has then been extended to poly-dispersed spheres by Soulié et al. (2006) and expanded herein through integrating the liquid bridge volume for mean pore size in Eqs. 19, 20 (Fig. 3).

$$F_{\text{cap}} = \pi \times T_s \times \sqrt{R_1 \times R_2} \cdot \left[c + \exp\left(a\frac{D}{R_2} + b\right)\right] = \pi \cdot T_s \cdot \sqrt{\left(\frac{D_{50}}{2}\right)^2} \cdot \left[c + \exp\left(a \times d_{\text{pore}} \times \frac{2}{D_{50}} + b\right)\right] \tag{15}$$

where

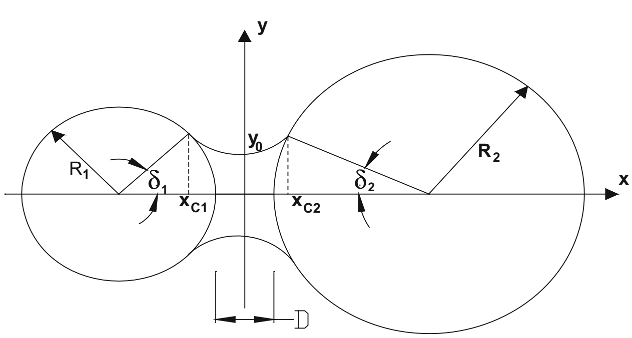

Fig. 3 Liquid bridge geometry between pair of quartz spheres

$$a = -1.1 \times \left(\frac{V}{R_2^3}\right)^{-0.53} = -1.1 \times \left(V \div \left(\frac{D_{50}}{2}\right)^3\right)^{-0.53} \tag{16}$$

$$b = \left(-0.148\ln\left(\frac{V}{R_2^3}\right) - 0.96\right)\Theta^2 - 0.0082\ln\left(\frac{V}{R_2^3}\right) + 0.48 = \left(-0.148\ln\left(V \div \frac{D_{50}{}^3}{2}\right) - 0.96\right) \times \Theta^2 - 0.0082\ln\left(V \div \frac{D_{50}{}^3}{2}\right) + 0.48$$

$$c = 0.0018\ln\left(\frac{V}{R_2^3}\right) + 0.078 = 0.0018\ln\left(V \div \frac{D_{50}{}^3}{2}\right) + 0.078 \tag{17}$$

$$V = 2R\left(\int_{x_{c1}}^{x_{c2}} y^2(x)\mathrm{d}x - 2s\right) = 2R \times \left\{\left[2\int_{-\left(R+\frac{D}{2}-\frac{(r_1+r_2)R\cos\delta}{R+\frac{D}{2}}\right)}^{\left(R+\frac{D}{2}-\frac{(r_1+r_2)R\cos\delta}{R+\frac{D}{2}}\right)} \int_0^{R\cdot\sin\delta} (x^2 + y^2 + A^2 - 2Ay - r_1^2)^2 \mathrm{d}y\mathrm{d}x\right]\right\} \tag{18}$$

where

$$s = \frac{\pi \cdot R^2}{360} \times 2\delta - \frac{R^2}{2} \cdot \sin 2\delta \tag{19}$$

$$A = (R + r_1) \cdot \sin\delta \tag{20}$$

$$\delta = \mathrm{Arccos}\left(\frac{R + \frac{D}{2}}{R + r_1}\right) \tag{21}$$

where Θ is the contact angle between the contractile skin [i.e. zero for pure water and glass after Fredlund and Rahardjo (1993) and between clean quartz grains], r_2 is the internal radius of the principal curvature, and r_1 is the external radius, which was estimated from the Laplace equation (Eq. 22).

$$(U_a - U_w)_p = T_s \times \left(\frac{1}{r_1} - \frac{1}{r_2}\right) \tag{22}$$

Model validity

For this study, particles are assumed mono-dispersed ($d = d_{50}$), spherical in shape, incompressible and non-crushable. The poorly graded PMs with the pronounced mode on 10–20 μm lend a good degree of credibility to the incompressibility and integrity of quartz constituents in the absence of an external high-energy load (Assadi et al. 2014). Forces operate on grain–grain contact points and flow through columns of grains that are aligned into load-carrying paths (Fig. 2). Forces were approximated at the mid-height of the testing soil column. Despite appreciating the fact that water front moves within the pore network through preferred water paths (Assadi and Yasrobi 2012), given the closely controlled deposition conditions an even distribution of water was speculated. Because tangential forces contribute to skeletal stresses only to a limited extent (Cundall and Strack 1979), their impact together with the impact of contact moments was neglected in calculations. Concurring with Santamarina (2003) general argument on minimal damping of force in angular grain assemblies, the sub-angular texture of PMs used justified our assumption of zero damping of force across the specimen.

Results and discussion

The free oedometer experiments as detailed in 'Testing procedures' section allowed the approximation of inter-particle forces for a range of degrees of saturation (associated with matric suction via a wetting-protocol filter paper test). The procedure might be argued to be practical due to the complexity in acquiring identical undisturbed soil specimens, although this drawback can be relaxed by geophysical profiling (Noborio 2001).

A suite of graphs are presented in this section including the measured wetting timed trend of void ratio and inter-particle forces for the testing calcareous reworked dust specimen (Fig. 4). In the first place, the graphs inform the reader in understanding the structural collapse at the grain scale, i.e. the destruction of reworked metastable structure upon wetting, which stands for the threshold of deflation when wind force exceeds capillary–cementation bond forces combined. Also, the graphs inform the reader of the reliance of collapse to the total destabilising Newtonian inter-particle force. Key question in this context is: What is the major cause of reworked dust structural destabilisation at elevated levels of inter-particle forces: A drop in the tensile capillary force or the modification of chemical cementation?

Capillary force initially increased with the advancement of waterfront (Fig. 5), while destabilising inter-particle force ($F_{(N)\text{skel}} - D + W + U - B$) also increased to its peak and dropped thereafter (Fig. 6). Structural collapse was captured at a 42 % degree of saturation when the total destabilising inter-particle force (deviatory stress at grain level) exceeded the capillary and cementation forces combined and sheared the cemented structure. During the wetting process, collapse was captured before capillary and destabilising forces reached their maximum. Chemical cementation was inferred to play a key role in domains

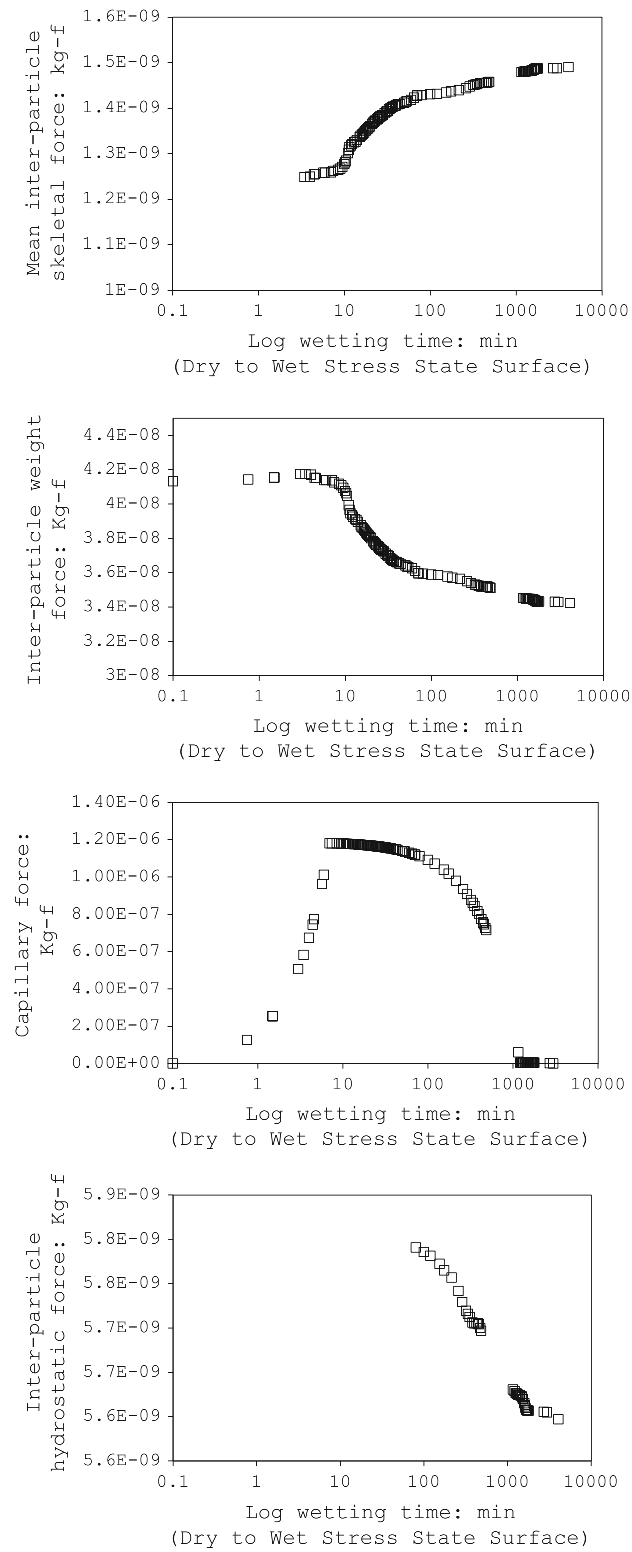

Fig. 4 Variation of inter-particle forces on the dry-to-wet stress-state surface

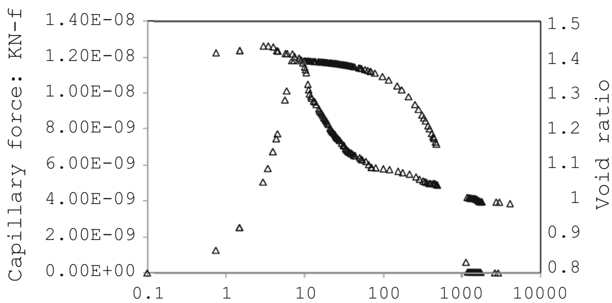

Fig. 5 Timed variation of water tension and void ratio upon wetting

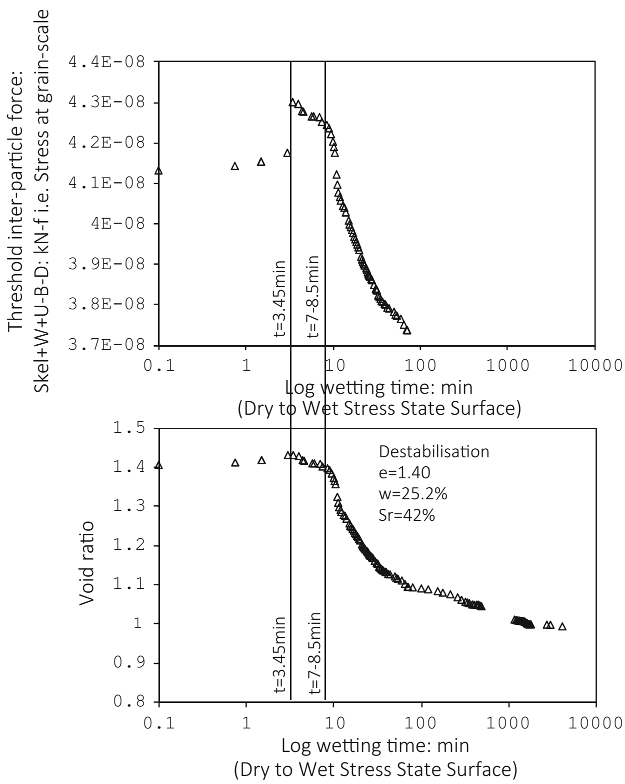

Fig. 6 Timed variation of cohesive inter-particle forces (balanced destabilising inter-particle forces) upon wetting

volumetric change, a more significant role than that played by capillary in retaining the dust structure over the wetting course. The measured capillary force immediately before collapse was approximately four times less than the total destabilising inter-particle force, lending further evidence to the significance of chemical cementation in retaining the open-packed domain. Cementation in Fig. 6 appears in the captured hardening response of specimen. The drop in totalled inter-particle force was initially followed by constant volumetric strain (function of void ratio), lending a brittle hardening feature to the material. The greater significance of cementation forces than capillary forces lends credibility to (1) the greater risk of deflation in modern reworked soil with climate gaining more extreme patterns, (2) suitability of an array of 'surface armouring' to stabilise reworked dust accumulations including bacterial communities, e.g. cyanobacteria, in the presence of sufficient sources of free calcium ions (Svirčev et al. 2013).

Conclusion

Deposition and deflation of airborne dust is an emerging global challenge in the light of predicted stronger aridity and winds within current climatic scenarios. Wind soil erosion and formation of dust plums have health and environmental implications, particularly at the margins of natural dust sources (e.g. Saharan and Sahel of North Africa) as well as modern dust sources. The controls on the trigger of dust deflation into the atmosphere are yet poorly known, particularly when particulate matters (silt-sized quartz) are combined with other minerals and develop a range of size distributions and inter-particle forces. There is a need, therefore, for these controls to be identified for the purpose of planning and implementing appropriate mitigation measures. Since deflation takes place for a mean surface wind force greater than soil cementation–capillary forces combined (i.e. fluid threshold), an estimation of particle-level forces is key to any dust flux trigger modelling attempt.

This paper described a semi-empirical model for estimation of inter-particle forces in loose aeolian fine silts with clay and carbonate inclusions. A suite of identical reworked dust specimens were simulated through wet aeolian deposition of clay-coated silts followed by cyclic wetting–drying chemical treatment to produce aragonite/calcite bonds. Benchmark specimen contained 70 % quartz silt (by weight) with a marked mode on 10–20 µm (PM_{10}), 20 % carbonate (<2 µm) and 10 % kaolinite (<2 µm)—not untypical of much of the earth's quaternary aerosols. For a range of water contents, inter-particle forces were approximated through logging the mean particle and pore size, mean hydraulic head, matric suction, void ratio and ambient conditions. Temporal bonding forces supplied by secondary reprecipitated carbonates were observed to be four times that of capillary forces, playing the primary role in maintaining the open and loosely cemented dust domains.

Acknowledgments This project was partially supported by 2654 Action 2 - Lot 16b EU grant with additional support with facilities through the European Regional Development Fund (ERDF). We also appreciate the assistance of staff at the School of Geography, University of Lecesiter for helping with Laser Diffraction Spectrometry analysis and the staff at Civil Engineering and Geosciences school, Newcastle University for their helpful comments through the invited talk delivered at the GEST seminar series.

References

Alfaro SC, Gaudichet A, Gomes L, Maille M (1998) Mineral aerosol production by wind erosion: aerosol particle sizes and binding energies. Geophys Res Lett 25:991–994

Andrade JE, Tu X (2009) Multiscale framework for behavior prediction in granular media. Mech Mater 41:652–669

Arya LM, Paris JF (1981) A physicoempirical model to predict the soil moisture characteristic from particle-size distribution and bulk density data. Soil Sci Am J 45:1023–1030

Arya LM, Paris JF (1982) Reply to comments on: A physicoempirical model to predict the soil moisture characteristic from particle-size distribution and bulk density data. Soil Sci Soc Am J 46:1348–1349

Arya LM, Leij FJ, Van Genuchten MT, Shouse PJ (1999) Scaling parameter to predict the soil water characteristic from particle-size distribution data. Soil Sci Soc Am J 63:210–519

Assadi A (2014) Micromechanics of collapse in loess. The University of Birmingham, Birmingham

Assadi A, Jefferson I (2013) Collapsibility in calcareous clayey loess: a factor of stress-hydraulic history. Int J GEOMATE 5(1):620–627

Assadi A, Yasrobi SS (2012) Drainage controlled uniaxial swelling cell. In: Proceedings of the ICE—geotechnical engineering, vol 166

Assadi A, Jefferson I, O'Hara-Dhand K, Smalley I (2014) Micromechanics of quartz sand breakage in a fractal context. Geomorphology 211:1–10

Assallay AM (1998) Structure and hydrocollapse behaviour of loess. Loughborough University, Loughborough

ASTM (2014) D4546-14 standard test methods for one-dimensional swell or collapse of soils

Bagnold RA (1941) The physics of blown sand and desert dunes. Methuen, New York

Bear J (1972) Dynamics of fluids in porous media. Dover, New York

BS (1990) BS 1377-5:1990 methods of test for soils for civil engineering purposes. Compressibility, permeability and durability tests

Claudin P, Bouchaud JP, Cates ME, Wittmer JP (1998) Models of stress fluctuations in granular media. Phys Rev E 57:4441–4457

Cornelis WM, Gabriels D, Hartmann R (2004) A parameterisation for the threshold shear velocity to initiate deflation of dry and wet sediment. Geomorphology 59:43–51

Creyssels M, Dupont P, Ould el Moctar A, Valance A, Cantat I, Jenkins JT, Pasini JM, Rasmussen KR (2009) Saltating particles in a turbulent boundary layer: experiment and theory. J Fluid Mech 625:47–74

Cundall PA, Strack ODL (1979) Discrete numerical-model for granular assemblies. Geotechnique 29:47–65

Cundall PA, Strack ODL (1983) Modelling of microscopic mechanisms in granular material. In: Jenkins JT, Satake M (eds) US–Japan seminar on new models and constitutive relationships in the mechanics of granular materials

Dantu P (1957) Contribution a l'etude mecanique et geometrique des milieux pulverulents. In: 4th international conference of soil mechanics, pp 144–148

Fredlund DG, Rahardjo H (1993) Soil mechanics for unsaturated soils. Wiley, London

Ginoux P, Prospero JM, Torres O, Chin M (2004) Long-term simulation of global dust distribution with the GOCART model: correlation with North Atlantic Oscillation. Environ Model Softw 19(2):113–128

Goossens D (2004) Effect of soil crusting on the emission and transport of wind-eroded sediment: field measurement on loamy soil. Geomorphology 58:145–160

Graf WH (1984) Hydraulics of sediment transport. Water Resources Publications, Highlands Ranch

Guo N, Zhao J (2013) The signature of shear-induced anisotropy in granular media. Comput Geotech 47:1–15

Harireche O, Faramarzi A, Alani AM (2013) A toroidal approximation of capillary forces in polydisperes granular assemblies. Granular matter 15:573–581

Haverkamp R, Parlange (1982) Comments on: A physicoempirical model to predict the soil moisture characteristic from particle-size distribution and bulk density data. Soil Sci Soc Am J 46:1348–1349

Ishizuka M, Mikami M, Leys J, Yamada Y, Heidenreich S, Shao Y, McTainsh GH (2008) Effects of soil moisture and dried raindroplet crust on saltation and dust emission. J Geophys Res 113:D24212

Lamb H (1994) Hydrodynamics. Trinity College, Cambridge University Press, Cambridge

Maher BA, Prospero JM, Mackie D, Gaiero D, Hesse PP, Balkanski Y (2010) Global connections between aeolian dust, climate and ocean biogeochemistry at the present day and at the last glacial maximum. Earth Sci Rev 99:61–97

Marticorena B, Bergametti G, Callot Aumont B, N'Doume C, Legrand M (1997) Modelling the atmospheric dust cycle 2. Simulation of Saharan dust sources. J Geophys Res 102(D4):4387–4404

Mikami T, Kamiya H, Horio M (1998) Numerical simulation of cohesive powder behavior in a fluidized bed. Chem Eng Sci 53:1927–1940

Miller RL, Tegen I, Perlwitz J (2004) Surface radiative forcing by soil dust aerosols and the hydrologic cycle. J Geophys Res Atmos 109(D4):1–24

Noborio K (2001) Measurement of soil water content and electrical conductivity by time domain reflectometry: a review. Comput Electron Agric 31:213–237

O'Hara-Dhand K, Assadi A, Jefferson I, Smalley I (2013) The control of loess grain shape on size distribution data. In: Neild J, Wilson R (eds) 19th Windy Day: UK aeolian research community meeting, University of Southampton

Ostojic S, Somfai E, Nienhuis B (2006) Scale invariance and universality of force networks in static granular matter. Nature 439:828–830

Ravi S, Zobeck TM, Over TM, Okin GS, D'Odorico P (2006) On the effect of moisture bonding forces in air-dry soils on threshold friction velocity of wind erosion. Sedimentology 53:597–609

Santamarina JC (2003) Soil behavior at the microscale: particle forces. In: Germaine JT, Sheahan TC, Whitman RV (eds) Soil behavior and soft ground construction. Geotechnical Special Publication. American Society of Civil Engineers, New York, pp 25–56

Shao Y et al (2011) Dust cycle: an emerging core theme in Earth system science. Aeolian Res 2:181–204

Smalley IJ (1970) Cohesion of small particles and the intrinsic resistance of simple soil systems to wind erosion. J Soil Sci 21:154–161

Soulié F, Cherblanc F, El Youssoufi MS, Saix C (2006) Influence of liquid bridges on the mechanical behaviour of polydisperse granular materials. Int J Numer Anal Methods Geomech 30:213–228. doi:10.1002/nag.476

Svirčev Z et al (2013) Importance of biological loess crusts for loess formation in semi-arid environments. Quat Int 296:206–215

Thornton C, Barnes DJ (1986) Computer simulated deformation of compact granular assemblies. Acta Mech 64:45–61

USEPA (2013) Particulate matter (PM). United States Environmental Protection Agency